

Enhanced ferromagnetism and conductivity of ultrathin freestanding $La_{0.7}Sr_{0.3}MnO_3$ membranes

Siqi Shan(单思齐), Yequan Chen(陈业全), Yongda Chen(陈勇达), Wenzhuo Zhuang(庄文卓), Ruxin Liu(刘汝新), Xu Zhang(张旭), Rong Zhang(张荣), and Xuefeng Wang(王学锋)
Citation: Chin. Phys. B, 2023, 32 (**10**): 107402. DOI: 10.1088/1674-1056/ace161
Journal homepage: http://cpb.iphy.ac.cn; http://iopscience.iop.org/cpb

What follows is a list of articles you may be interested in

Multiple surface states, nontrivial band topology, and antiferromagnetism in $GdAuAl_4Ge_2$

Chengcheng Zhang(张成成), Yuan Wang(王渊), Fayuan Zhang(张发远), Hongtao Rong(戎洪涛), Yongqing Cai(蔡永青), Le Wang(王乐), Xiao-Ming Ma(马小明), Shu Guo(郭抒), Zhongjia Chen(陈仲佳), Yanan Wang(王亚南), Zhicheng Jiang(江志诚), Yichen Yang(杨逸尘), Zhengtai Liu(刘正太), Mao Ye(叶茂), Junhao Lin(林君浩), Jiawei Mei(梅佳伟), Zhanyang Hao(郝占阳), Zijuan Xie(谢子娟), and Chaoyu Chen(陈朝宇)
Chin. Phys. B, 2023, 32 (**7**): 077401. DOI: 10.1088/1674-1056/acca0e

Superconductivity in self-flux-synthesized single crystalline $R_2Pt_3Ge_5$(R = La, Ce, Pr)

Q Sheng(盛琪), J Zhang(张建), K Huang(黄百畅), Z Ding(丁兆峰), X Peng(彭小冉), C Tan(谭程), L Shu(殳蕾)
Chin. Phys. B, 2017, 26 (**5**): 057401. DOI: 10.1088/1674-1056/26/5/057401

First-principles calculation of the structural,electronic,and magnetic properties of cubic perovskite RbXF$_3$(X=Mn,V,Co,Fe)

Muhammad Raza ur rehman Hashmi, Muhammad Zafar, M Shakil, Atif Sattar, Shabbir Ahmed, S A Ahmad
Chin. Phys. B, 2016, 25 (**11**): 117401. DOI: 10.1088/1674-1056/25/11/117401

Theoretical investigations of half-metallic ferromagnetism in new Half—Heusler YCrSb and YMnSb alloys using first-principle calculations

M Atif Sattar, Muhammad Rashid, M Raza Hashmi, S A Ahmad, Muhammad Imran, Fayyaz Hussain
Chin. Phys. B, 2016, 25 (**10**): 107402. DOI: 10.1088/1674-1056/25/10/107402

High-pressure studies on heavy fermion systems

Ye Chen(陈晔), Zongfa Weng(翁宗法), Smidman Michael, Xin Lu(路欣), Huiqiu Yuan(袁辉球)
Chin. Phys. B, 2016, 25 (**7**): 077401. DOI: 10.1088/1674-1056/25/7/077401

Enhanced ferromagnetism and conductivity of ultrathin freestanding $La_{0.7}Sr_{0.3}MnO_3$ membranes

Siqi Shan(单思齐), Yequan Chen(陈业全), Yongda Chen(陈勇达), Wenzhuo Zhuang(庄文卓), Ruxin Liu(刘汝新), Xu Zhang(张旭), Rong Zhang(张荣), and Xuefeng Wang(王学锋)†

Jiangsu Provincial Key Laboratory of Advanced Photonic and Electronic Materials, School of Electronic Science and Engineering, and Collaborative Innovation Center of Advanced Microstructures, Nanjing University, Nanjing 210093, *China*

(Received 9 June 2023; revised manuscript received 9 June 2023; accepted manuscript online 25 June 2023)

We report a universal method to transfer freestanding $La_{0.7}Sr_{0.3}MnO_3$ membranes to target substrates. The 4-unit-cell-thick freestanding $La_{0.7}Sr_{0.3}MnO_3$ membrane exhibits the enhanced ferromagnetism, conductivity and out-of-plane magnetic anisotropy, which otherwise shows nonmagnetic/antiferromagnetic and insulating behavior due to the intrinsic epitaxial strain. This work facilitates the promising applications of ultrathin freestanding correlated oxide membranes in electronics and spintronics.

Keywords: freestanding membranes, $La_{0.7}Sr_{0.3}MnO_3$, ferromagnetism, magnetic anisotropy

PACS: 74.78.Fk, 75.30.Gw, 75.47.Lx, 75.70.–i **DOI:** 10.1088/1674-1056/ace161

The rapid development of flexible electronics successively provides new multifunctional smart wearable electronic devices, which are gradually changing daily life.[1–4] The miniaturization, flexibility, integration and low power consumption of wearable devices have increasingly required functional materials, especially correlated oxide materials, in which the d-orbital electrons are highly correlated with the charge, spin, orbital, and lattice degrees of freedom.[5–7] The critical interaction among these four degrees of freedom leads to novel quantum phenomena, such as high-temperature superconductivity,[8–10] colossal magnetoresistance,[11,12] metal-insulator phase transition,[13,14] and multiferroics.[15–18] In recent years, relying on the controllable film growth and effective transfer technologies, freestanding (FS) single-crystalline correlated oxide membranes have been obtained.[19–22] When membranes are stripped from the substrates, the intrinsic epitaxial strain of the films is fully relaxed, showing rich magnetism,[22–24] electrical properties[14,25] and ferroelectricity.[26–28] These FS membranes could find a wide range of applications in information storage, intelligent sensing, and energy, etc.

As a typical correlated oxide, $La_{0.7}Sr_{0.3}MnO_3$ (LSMO) has attracted great interest due to its high Curie temperature (T_C) ($\sim$369 K), large spin polarization,[29] and colossal magnetoresistance.[11,30] FS-LSMO membranes were firstly reported by etching water-soluble $Sr_3Al_2O_6$ (SAO) sacrificial layer in 2016,[19] in which the hysteresis loop was observed in the 20-nm-thick membranes. Until now, ferromagnetism has been observed in FS-LSMO membranes with the thickness ranging from 20 to 88 nm, which were transferred via dissolving various sacrificial layers (e.g., SAO, $SrRuO_3$, and $SrCoO_{2.5}$).[18,23,31–33] However, the transport properties of ultrathin (less than 10 nm) FS-LSMO membranes still remain largely unexplored due to the extreme difficulty in obtaining the intact transferred sample.

In this work, we experimentally demonstrate a universal and effective methodology to transfer large-area and single-crystalline FS-LSMO membranes onto any target substrates. The LSMO films and SAO sacrificial layers are deposited on $SrTiO_3$ (STO) substrates by pulsed laser deposition (PLD). Enhanced ferromagnetism and conductivity of the ultrathin FS-LSMO membranes are both observed. The saturated magnetic moment (M_S) of 4-unit-cell (u.c.)-thick FS-LSMO membranes is as high as 2.19 μ_B/Mn at 15 K. Moreover, it shows the out-of-plane magnetic anisotropy. This work provides a feasible route to fabricate flexible LSMO-based oxide spintronic devices compatible with conventional semiconductor technologies.

We firstly deposited 40-nm-thick SAO sacrificial layers and LSMO films with the thickness ranging from 4 to 120 u.c. on the (001)-STO substrates [as schematically shown in Fig. 1(a)] by the PLD, which was monitored by reflected high-energy electron diffraction (RHEED) oscillations.[24,34,35] The SAO layers were deposited on the STO (001) substrates ($5 \times 5 \times 0.5$ mm^3) at 750 °C under the oxygen pressure of 10^{-5} mbar. Then, LSMO films with varied thickness were deposited at 700 °C under the oxygen pressure of 10^{-4} mbar. The relative low partial oxygen pressure ensured the high quality of the grown SAO sacrificial layer. The deposition temperature of LSMO films was precisely controlled at 700 °C to avoid the extra interfacial reaction between LSMO and SAO.[20] After growth, the samples were cooled down to room temperature at a rate of 10 °C/min without changing the oxygen pressure. The surface morphology and thickness of the membranes were

†Corresponding author. E-mail: xfwang@nju.edu.cn

© 2023 Chinese Physical Society and IOP Publishing Ltd

examined by means of an atomic force microscope (AFM) system (Asylum Cypher). The crystalline structure was examined by a high-resolution x-ray diffraction (XRD, Bruker D8 Discover). The incident x-ray was generated from Cu K_α emission and had a wavelength of 1.5418 Å. A Quantum Design superconducting quantum interference device magnetometer (SQUID) system of up to 9 T was employed to measure magnetic properties. A cryogen free measurement system (CFMS, Cryogenic) was employed to characterize the transport properties at temperatures from 1.6 K to 300 K in a magnetic field (up to 12 T).

The clear RHEED oscillations indicate the 2D layer-by-layer epitaxial growth of 4- and 12-u.c.-thick LSMO ultrathin films, respectively (see Fig. S1 in the supplementary material). A 120-u.c.-thick LSMO film was also prepared. Its thickness was estimated by the deposition time, as confirmed by AFM (see Fig. S2 in the supplementary material). To avoid the potential reaction at the interface between LSMO and SAO, the deposition temperature of the LSMO films was kept at 700 °C.[36]

After growth, a poly-dimethylsiloxane (PDMS) supporting layer was stamped onto the clean surface of the heterostructure. The whole sample with PDMS was immersed in deionized water to etch the SAO sacrificial layer [Fig. 1(b)]. After the SAO sacrificial layer was fully etched, the LSMO film was exfoliated [Fig. 1(c)]. Subsequently, the LSMO film was transferred onto a clean silicon substrate [Fig. 1(d)] and heated to 120 °C to remove PDMS supporting layer [Fig. 1(e)]. Finally, the FS-LSMO membranes was attached on the silicon substrates, forming new strain-free heterostructures [Fig. 1(f)]. This transfer methodology has been applied to other correlated oxides and topological materials.[19,37]

Figure 1(g) displays the corner of a 12-u.c.-thick FS-LSMO membrane, which manifests the integrality of the membrane. The XRD patterns of 12-u.c.-thick LSMO before (black curve) and after (red curve) transfer are shown in Fig. 1(h). The diffraction peaks correspond to (002) planes, indicating the single-crystalline epitaxial growth along the c axis. A slight shift of the diffraction peak towards the lower angle is observed after transfer, suggesting a decrease in in-plane lattice constant of the LSMO membrane. According to the lattice constants of STO and LSMO (3.905 Å and 3.875 Å, respectively), the peak shift of the XRD pattern implies the relaxed tensile strain of the LSMO lattice in the FS-membrane. The XRD patterns of another 12-u.c.-thick LSMO sample are also provided (see Fig. S3 in the supplementary material), which is deposited on a $(LaAlO_3)_{0.3}(Sr_2AlTaO_6)_{0.7}$ (LSAT) substrate. The peak shift of the XRD patterns shows the opposite trend. Obviously, the in-plane lattice constant of LSMO increases after transfer, which is attributed to the smaller lattice constant of LSAT (3.868 Å).

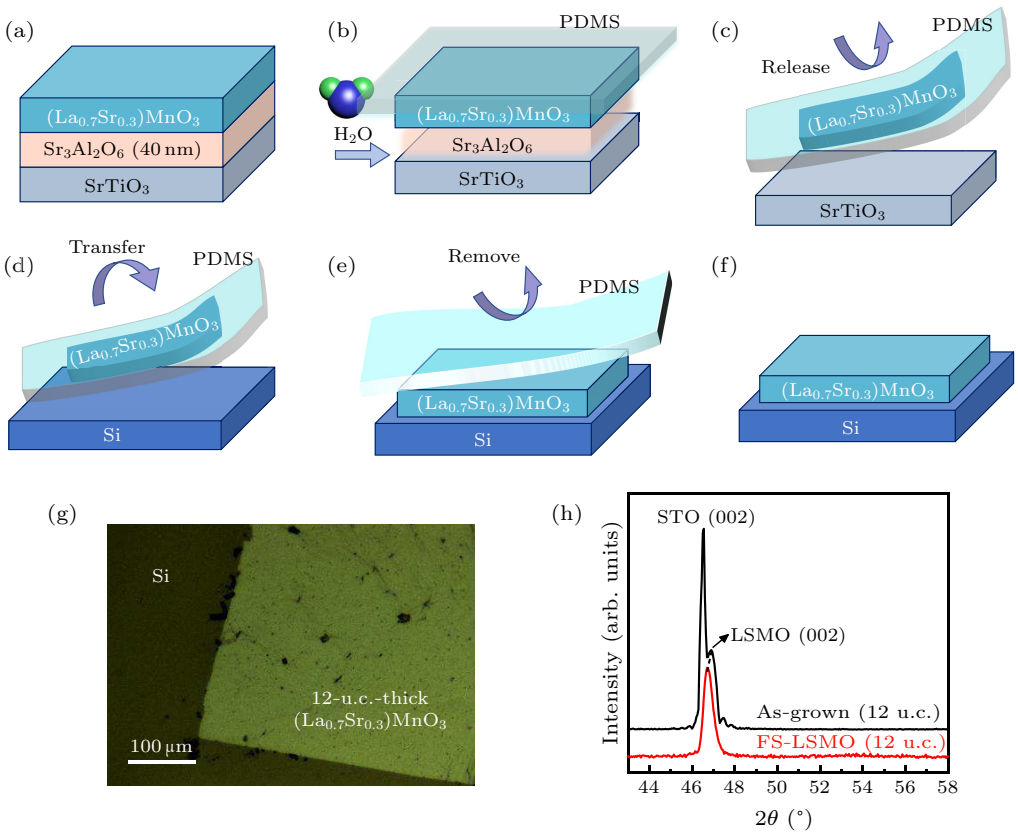


Fig. 1. (a)–(f) Schematic illustration of the release and transfer process of the ultrathin FS-LSMO membranes. (g) Photograph of transferred FS-LSMO membranes with thickness of 12 u.c. on Si. (h) XRD patterns of the LSMO (12 u.c.) before and after transfer, respectively.

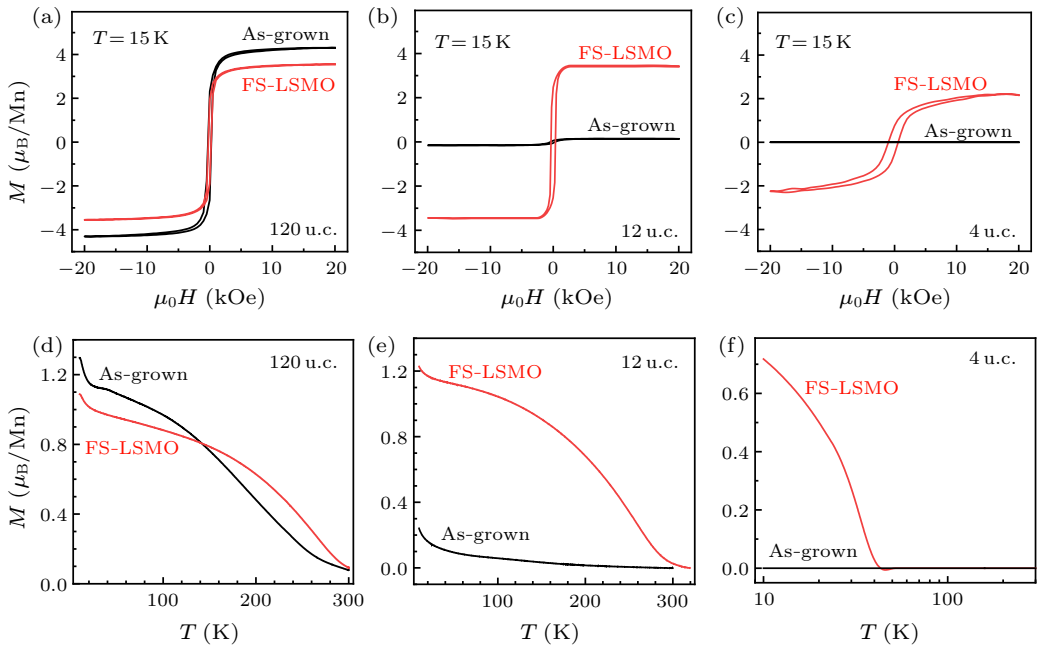


Fig. 2. The magnetic properties of LSMO films with different thicknesses before and after transfer. (a)–(c) Magnetic hysteresis loops of LSMO films before (black curve) and after (red curve) transfer at 15 K, respectively. (d)–(f) Temperature-dependent magnetization curves of LSMO films before (black curve) and after (red curve) transfer under 100 Oe, respectively. The magnetic field is applied perpendicular to the substrates.

Table 1. The T_C of LSMO films and membranes with thicknesses of 120, 12, and 4 u.c., respectively.

Thickness of LSMO	120 u.c.	12 u.c.	4 u.c.
T_C of LSMO epitaxial films	185.5 K	127.6 K	–
T_C of FS-LSMO membranes	266.8 K	258.1 K	32.3 K

Next, we investigate the magnetic properties of the LSMO films before and after transfer under the out-of-plane magnetic field. With the decreasing thickness of LSMO films, the ferromagnetism is gradually suppressed, as seen from the black curves in Fig. 2. The 4-u.c.-thick LMSO film before transfer is generally considered to be less than the dead layer thickness. It shows the nonmagnetic/antiferromagnetic property, which is in line with the previous work.[24,38] After transfer, the 120- and 12-u.c.-thick FS-LSMO membranes maintain ferromagnetism at 15 K with the opposite trend. The saturation magnetic moment (M_S) of 120-u.c.-thick LSMO membranes decreases from 4.31 μ_B/Mn to 3.55 μ_B/Mn while the M_S of 12-u.c.-thick LSMO increases from 0.14 μ_B/Mn to 3.44 μ_B/Mn. This is ascribed to the different strain relaxation in the LSMO membranes. Specifically, the epitaxial strain of the 120-u.c.-thick LSMO is fully relaxed even before transfer. The degradation of the M_S is due to the inevitable folding of the membranes during the transfer. On the other hand, the transfer process relaxes the epitaxial strain in the 12-u.c.-thick film, which leads to the obvious increase of M_S. The T_C values are determined by plotting the derivative of the temperature-dependent magnetization (M–T) curves under 100 Oe [Figs. 2(d)–2(f) and Fig. S4 of the supplementary material], as summarized in Table 1. The T_C increases about 81.3 K and 130.5 K for 120- and 12-u.c.-thick FS-LSMO membranes after transfer, respectively. Remarkably, a prominent transition to ferromagnetism with M_S of 2.19 μ_B/Mn and T_C of 32.3 K is observed in the 4-u.c.-thick FS-LSMO membranes [Figs. 2(c) and 2(f)], which is attributed to the full relaxation of the epitaxial strain.

The dead-layer effect has also led to the degradation of the conductivities in LSMO ultrathin films.[38,39] Here, the transport properties of the 4-u.c.-thick LSMO films before and after transfer were successfully measured via the standard six-probe method. The insulating property of the 4-u.c.-thick LSMO films is expected according to the temperature-dependent resistivity curves [black squares in Fig. 3(a)]. Remarkably, the 4-u.c.-thick intact FS-LSMO membranes show the well-defined metallic behavior after transfer [red circles in Fig. 3(a)], which has never been seen before. However, the separation of the insulator-metal transition temperature (T_{IM}, higher than 300 K) and the T_C can be attributed to the different impacts on the microstructures and Mn^{3+}/Mn^{4+} ratio during transfer process.[40] The magnetoresistance (MR) of 4-u.c.-thick FS-LSMO membranes under the out-of-plane magnetic field is further measured at 5 K and 10 K, which is defined as $[R_{xx}(H) - R_{xx}(0)]/R_{xx}(0)$. The MR is negative and exhibits distinct symmetrical humps around origin at both 5 K and 10 K [Fig. 3(b)]. It suggests that the disordered structure of magnetic domains generates when the magnetic field is reduced to the coercivity (H_C). Such magnetic domains in LSMO membranes are further aligned under a large magnetic field, which is generally considered as butterfly shaped behavior in previous studies.[23,24,41] Thus, the butterfly-shaped MR is manifested, further verifying the ferromagnetism of the 4-

u.c.-thick FS-LSMO membranes.

Figure 4(a) shows the normalized hysteresis loops of 4-u.c.-thick FS-LSMO membranes at 15 K under in-plane and out-of-plane magnetic field, respectively. The magnetic easy-axis significantly lies towards in-plane alignment due to the smaller H_C and the lower saturation field. The standard angle-dependent $[R_{xx}(\theta) - R_{xx}(0)]/R_{xx}(0)$ curves under 6 T at 5 K and 300 K are shown in Fig. 4(b), where θ is defined as the angle between the external magnetic field and the c-axis of LSMO membranes. The magnetic easy axis can be directly distinguished at $\theta = 120°$ at both 5 K and 300 K, which prefers to an in-plane alignment. The magnetic easy-axis of LSMO can be modulated from the out-of-plane to the in-plane direction according to the interfacial strain.[35,42] However, the canted easy-axis of ultrathin 4-u.c. FS-LSMO membrane may be attributed to the stress induced by the transfer process instead of epitaxial strain, which is fully released. The clear angular symmetry of the $[R_{xx}(\theta) - R_{xx}(0°)]/R_{xx}(0°)$ curves in the 4-u.c.-thick FS-LSMO membranes further manifests the high quality of the transferred FS-membranes.

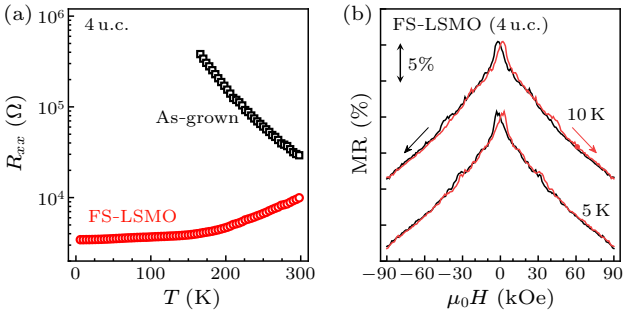


Fig. 3. (a) Temperature-dependent resistance curves of LSMO films before and after transfer, respectively. (b) The field-dependent MR curves of LSMO membranes measured at 5 K and 10 K, respectively.

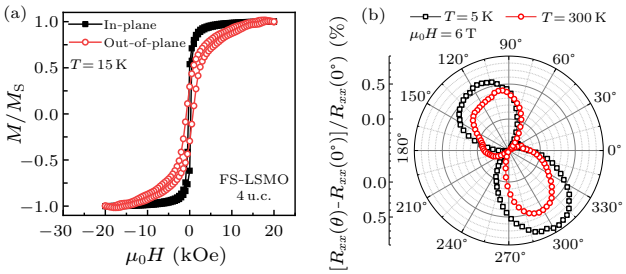


Fig. 4. Magnetic anisotropy of the 4-u.c.-thick FS-LSMO membranes. (a) In-plane and out-of-plane magnetic hysteresis loops at 15 K. (b) The angular dependence of $[R_{xx}(\theta) - R_{xx}(0)]/R_{xx}(0)$ curves at 5 K and 300 K, respectively.

In summary, we have demonstrated a universal method to transfer FS-LSMO membranes with various thicknesses onto silicon substrates, which maintains the high quality as well as the enhanced electrical and magnetic properties. Notably, the obvious ferromagnetism and metallicity are observed in the ultrathin 4-u.c.-thick FS-LSMO membranes, whose thickness is generally less than the thickness of dead layers. This anomalous behavior can be mostly ascribed to the fully released epitaxial strain after transfer. Our work paves a pathway to make ultrathin manganite membranes compatible with the relevant semiconductor technologies. This transfer technique has promising applications in flexible oxide electronic and spintronic devices.

Acknowledgments

This work was supported in part by the National Key R&D Program of China (Grant No. 2022YFA1402404) and the National Natural Science Foundation of China (Grant Nos. 62274085, 11874203, and 61822403).

References

[1] Yao G, Kang L, Li J, Long Y, Wei H, Ferreira C A, Jeffery J J, Lin Y, Cai W B and Wang X D 2018 *Nat. Commun.* **9** 5349

[2] Long Y, Wei H, Li J, Yao G, Yu B, Ni D L, Gibson A L F, Lan X L, Jiang Y D, Cai W B and Wang X D 2018 *ACS Nano* **12** 12533

[3] Kim J, Son D, Lee M, Song C, Song J K, Koo J H, Lee D J, Shim H J, Kim J H, Lee M, Hyeon T and Kim D H 2016 *Sci. Adv.* **2** e1501101

[4] Baek S H, Park J, Kim D M, Aksyuk V A, Das R R, Bu S D, Felker D A, Lettieri J, Vaithyanathan V, Bharadwaja S S N, Bassiri-Gharb N, Chen Y B, Sun H P, Folkman C M, Jang H W, Kreft D J, Streiffer S K, Ramesh R, Pan X Q, Trolier-McKinstry S, Schlom D G, Rzchowski M S, Blick R H and Eom C B 2011 *Science* **334** 958

[5] Hwang H Y, Iwasa Y, Kawasaki M, Keimer B, Nagaosa N and Tokura Y 2012 *Nat. Mater.* **11** 103

[6] Mele P, Endo T, Arisawa S, Li C and Tsuchiya T 2015 *Oxide Thin Films, Multilayers, and Nanocomposites* (Berlin: Springer) p. 157

[7] Christensen D V, Trier F, Niu W, Gan Y L, Zhang Y, Jespersen T S, Chen Y Z and Pryds N 2019 *Adv. Mater. Interfaces* **6** 1900772

[8] Reyren N, Thiel S, Caviglia A D, Kourkoutis L F, Hammerl G, Richter C, Schneider C, Kopp T, Rüetschi A S, Jaccard D, Gabay M, Muller D A, Triscone J M and Mannhart J 2007 *Science* **317** 1196

[9] Gozar A, Logvenov G, Kourkoutis L F, Bollinger A T, Giannuzzi L A, Muller D A and Bozovic I 2008 *Nature* **455** 782

[10] Chen Z, Liu Z R, Sun Y Q, Chen X X, Liu Y, Zhang H, Li H K, Zhang M, Hong S Y, Ren T S, Zhang C, Tian H, Zhou Y, Sun J R and Xie Y W 2021 *Phys. Rev. Lett.* **126** 026802

[11] Wu Y, Suzuki Y, Rüdiger U, Yu J, Kent A D, Nath T K and Eom C B 1999 *Appl. Phys. Lett.* **75** 2295

[12] Jin K J, Lu H B, Zhou Q L, Zhao K, Cheng B L, Chen Z H, Zhou Y L and Yang G Z 2005 *Phys. Rev. B* **71** 184428

[13] Liao Z L, Li F M, Gao P, Li L, Guo J D, Pan X Q, Jin R, Plummer E W and Zhang J D 2015 *Phys. Rev. B* **92** 125123

[14] Han K, Wu L, Cao Y, Wang H Y, Ye C, Huang K, Motapothula M, Xing H N, Li X H, Qi D C, Li X and Wang X R 2021 *ACS Appl. Mater. Interfaces* **13** 16688

[15] Jia C L and Berakdar J 2009 *Appl. Phys. Lett.* **95** 012105

[16] Vaz C A F, Hoffman J, Ahn C H and Ramesh R 2010 *Adv. Mater.* **22** 2900

[17] Vaz C A F 2012 *J. Phys.: Condens. Matter* **24** 333201

[18] Pesquera D, Khestanova E, Ghidini M, Zhang S, Rooney A P, Maccherozzi F, Riego P, Farokhipoor S, Kim J, Moya X, Vickers M E, Stelmashenko N A, Haigh S J, Dhesi S S and Mathur N D 2020 *Nat. Commun.* **11** 3190

[19] Lu D, Baek D J, Hong S S, Kourkoutis L F, Hikita Y and Hwang H Y 2016 *Nat. Mater.* **15** 1255

[20] Baek D J, Lu D, Hikita Y, Hwang H Y and Kourkoutis L F 2017 *ACS Appl. Mater. Interfaces* **9** 54

[21] Ji D X, Cai S H, Paudel T R, Sun H Y, Zhang C C, Han L, Wei Y F, Zang Y P, Gu M, Zhang Y, Gao W P, Huyan H X, Guo W, Wu D, Gu Z B, Tsymbal E Y, Wang P, Nie Y F and Pan X Q 2019 *Nature* **570** 87

[22] Lu Q W, Liu Z W, Yang Q, Cao H, Balakrishnan P, Wang Q, Cheng L, Lu Y L, Zuo J M, Zhou H, Quarterman P, Muramoto S, Grutter A J, Chen H H and Zhai X F 2022 *ACS Nano* **16** 7580

[23] Zhang C, Ding S S, Qiao K M, Li J, Li Z, Yin Z, Sun J R, Wang J, Zhao T Y, Hu F X and Shen B G 2021 *ACS Appl. Mater. Interfaces* **13** 28442

[24] Chen Y D, Yuan X, Shan S Q, Zhang C, Liu R X, Zhang X, Zhuang W Z, Chen Y Q, Xu Y B, Zhang R and Wang X F 2022 *ACS Appl. Mater. Interfaces* **14** 39673

[25] Eom K, Yu M Q, Seo J, Yang D Y, Lee H, Lee J W, Irvin P, Oh S H, Levy J and Eom C B 2021 *Sci. Adv.* **7** eabh1284

[26] Lu D, Crossley S, Xu R J, Hikita Y and Hwang H Y 2019 *Nano Lett.* **19** 3999

[27] Xu R J, Huang J W, Barnard E S, Hong S S, Singh P, Wong E K, Jansen T, Harbola V, Xiao J, Wang B Y, Crossley S, Lu D, Liu S and Hwang H Y 2020 *Nat. Commun.* **11** 3141

[28] Jin C, Zhu Y M, Li X W, An F, Han W Q, Liu Q, Hu S X, Ji Y J, Xu Z D, Hu S B, Ye M, Zhong G K, Gu M and Chen L 2021 *Adv. Sci.* **8** 2102178

[29] Hemberger J, Krimmel A, Kurz T, Von Nidda H A K, Ivanov V Y, Mukhin A A, Balbashov A M and Loidl A 2002 *Phys. Rev. B* **66** 094410

[30] Ramirez A P 1997 *J. Phys.: Condens. Matter* **9** 8171

[31] Lu Z X, Liu J W, Feng J T, Zheng X, Yang L H, Ge C, Jin K J, Wang Z M and Li R W 2020 *APL Mater.* **8** 051105

[32] Wang H, Shen L K Lu L, Zhang B, Ma C R, Cao C M, Jiang C J, Liu M and Jia C L 2019 *IEEE Electron Dev. Lett.* **40** 1856

[33] Zhou W K, Han W Q, Yang Y H, Shu L, Luo Q G, Ji Y J, Jin C, Zhang Y L, Song J H, Ye M, Liu Q, Hu S B and Chen L 2023 *Appl. Phys. Lett.* **122** 062901

[34] Niu W, Gao M, Wang X F, Song F Q, Du J, Wang X R, Xu Y B and Zhang R 2016 *Sci. Rep.* **6** 26081

[35] Chen L M, Zhang C C, Chen Y Q, Chen Y D, Niu W, Wang P, Du J, Xu Y B, Zhang R and Wang X F 2019 *Appl. Phys. Lett.* **115** 201604

[36] Baek D J, Lu D, Hikita Y, Hwang H Y and Kourkoutis L F 2017 *APL Mater.* **5** 096108

[37] Chen Y Q, Liu R X, Chen Y D, Yuan X, Ning J A, Zhang C C, Chen L M, Wang P, He L, Zhang R, Xu Y B and Wang X F 2021 *Chin. Phys. Lett.* **38** 017101

[38] Chen H Y, Yu Y, Wang Z, Bai Y, Lin H X, Li X L, Liu H, Miao T, Kou Y F, Zhang Y S, Li Y, Tang J, Wang Z C, Cai P, Zhu Y Y, Cheng Z H, Zhong X Y, Wang W B, Gao X Y, Yin L F, Wu R Q and Shen J 2019 *Phys. Rev. B* **99** 214419

[39] Porter S B, Venkatesan M, Dunne P, Doudin B, Rode K and Coey J M D 2017 *IEEE Trans. Magn.* **53** 6000904

[40] Wu Y J, Ning X K, Wang Z J, Wang Q and Zhang Z D 2016 *J. Alloys Compd.* **667** 317

[41] Matou T, Takeshima K, Anh L D, Seki M, Tabata H, Tanaka M and Ohya S 2017 *Appl. Phys. Lett.* **110** 212406

[42] Ji H H, Yan Z, Zhou G W, Kang P H, Li Z L and Xu X H 2022 *J. Mater. Chem. C* **10** 12844